Available online at www.sciencedirect.com
SCIENCE DIRECT®
International Journal of Heat and Mass Transfer 47 (2004) 2619–2628
International Journal of HEAT and MASS TRANSFER
www.elsevier.com/locate/ijhmt

Heat transfer dynamics associated with the simultaneous growth of solid–liquid melt layers

Thirunavukarasu Bala, Deborah V. Pence, James A. Liburdy *

Department of Mechanical Engineering, Oregon State University, 204 Rogers Hall, Corvallis, OR 97331, USA

Received 28 July 2003; received in revised form 11 December 2003

Abstract

A computational model is developed to study the effects of alumina layer formation on an ablative surface, when exposed to high temperature particle laden gas flow. The one-dimensional model is developed taking into consideration the thermal loading, particle loading and the temperature dependence of the thermo-physical properties of alumina. A fully implicit finite volume method is used to solve the coupled set of non-linear heat conduction equations. The solidification interface is tracked using the Lagrangian interpolation technique. The particle mass flux was found to be the major factor affecting the solid layer growth rate and the heat transferred to the ablative layer. The gas heat flux also has a major effect on the solid growth rate and the heat transferred to the ablative surface, but only for the lower particle mass fluxes. On the other hand the particle temperature has a linear effect on the solidification dynamics and the heat transferred to the ablative surface for all particle mass fluxes. The heat transferred to the ablative surface is reduced by approximately 40–90%, depending on the mass fluxes, due to the formation of the alumina layer.

Keywords: Moving boundary; Expanding solution domain; Solidification; Melt layer

1. Introduction

Phase change phenomenon has been widely studied over the past several decades. Phase change problems with a moving boundary introduce the added complexity of resolving the interface position as an inherent part of the solution. A method for tracking this moving boundary in a fixed domain is given by Crank [1] and has been used by numerous researchers. A heat transfer situation with a moving boundary and simultaneous expanding domain is presented here. In this problem the domain expands due to mass influx and an internal moving interface is present due to phase change.

One area where this type of problem is of concern is in the design of missile canister launchers. When the missiles are launched from canisters the exhaust plumes impose severe thermal and surface erosion on the walls of the plenum and uptake regions. To protect the launchers from severe erosion, thick ablative liners are used to absorb the thermal load. The aluminum used to increase the performance of the solid propellant yields a two-phase exhaust plume consisting of molten alumina (Al_2O_3) and gaseous products of combustion. Some exhausts contain up to 40% by weight of alumina in the exhaust products [2]. The size distribution of the alumina, and the complex supersonic exhaust flow results in a range of local alumina number density impinging onto the ablative layer. As the molten alumina impinges on to the surface it forms a layer that, due to the ablative layer thermal response, quickly freezes. In the early phase of the missile launch the presence of alumina particles in the exhaust plume results in a high mechanical and thermal erosion of the ablative surface. Initially a solid alumina layer forms over the ablative surface. Later, as the solid alumina layer grows a melt layer begins to form, consequently the alumina becomes a complex

* Corresponding author. Tel.: +1-541-737-7017; fax: +1-541-737-2600.
E-mail address: liburdy@engr.oregonstate.edu (J.A. Liburdy).

0017-9310/$ - see front matter © 2004 Elsevier Ltd. All rights reserved.
doi:10.1016/j.ijheatmasstransfer.2003.12.012

Nomenclature

c_p	specific heat capacity of alumina, J/kg K
H	latent heat of solidification of alumina, J/kg
k	thermal conductivity of alumina, W/mK
L	instantaneous thickness of the alumina layer, m
L_{ref}	length reference, m
$\dot{m}''_p$	particle mass flux, kg/m^2 s
$\dot{m}''_s$	solidification rate of alumina, kg/m^2 s
$\dot{q}''_{ab}$	heat flux at the ablative surface/solid alumina interface, W/m^2
$\dot{q}''_{gas}$	gas heat flux, W/m^2
$\dot{q}''_s$	heat flux at the alumina/gas interface
$\dot{q}''_{S/L}$	heat flux at the solid/liquid alumina interface, W/m^2
$\dot{q}''_{KE}$	particle kinetic energy converted to thermal energy, W/m^2
$\dot{q}''_{part}$	particle thermal energy, W/m^2
$\dot{q}''_{lat}$	heat released from solidification, W/m^2
s	thickness of the solid alumina layer, m
t	time, s
t_{ref}	reference time, L^2_{ref}/α_o, s
T	temperature, K
T_a	fail temperature of the ablative surface, K
T_i	melting temperature of alumina, K
T_p	particle temperature, K
T_s	temperature of the alumina surface, K
Δt	time step, s
y	y-direction

Greek symbols

α	thermal diffusivity of alumina, m^2/s
δ	non-dimensional solid alumina layer thickness
δ_l	thickness of the liquid alumina layer, m
δ_n	thickness of the deposited alumina in each time step, m
δ_s	thickness of the solid alumina layer, m
δ_s/L	relative thickness of solid alumina layer
$\Delta\zeta$	non-dimensional spatial step, $\Delta y/L$
$\Delta\tau$	non-dimensional time step, $\Delta t/t_{ref}$
ζ	non-dimensional thickness of the alumina layer, $y/L(t)$
θ	non-dimensional temperature, $(T - T_a)/(T_p - T_a)$
ρ	density of alumina, kg/m^3
τ	non-dimensional time, t/t_{ref}

Subscripts

l	liquid alumina layer
o	properties evaluated at the reference temperature
s	solid alumina layer

structure of solid and liquid phases which protect the ablative layer from further mechanical and thermal erosion. The thermal load on the ablative layer decreases during the course of the missile launch due to the increasing thickness of the alumina layer. To incorporate design modifications to the existing missile launchers and to design future missile launchers, accurate estimates of these thermal loads during a missile launch is required. Improving the design of the existing launchers would increase the number of missiles that could be fired from a canister before ablator refurbishment and will help in launching high-impulse missiles from the canisters. Also, accurate heat transfer predictions are needed in the case of missile launch failure where by the ablative layer should be able to withstand the thermal loading throughout the motor burn.

The details of the two phase formation of this alumina layer and its effects on the surface heat transfer and ablation is still unresolved. This problem has been analyzed by a number of previous researchers who have allowed for a range of assumptions to simplify the problem. All of the previous models either under predicted or over predicted the limited experimental results of the ablation rate due to the assumptions made in the course of developing the model.

2. Previous models

Soo Hoo [3] developed a heat transfer model taking into consideration the particle kinetic energy and convective heating of the gas plume. He used a two-phase inviscid hydrocode to calculate the particle velocity and exhaust gas flow field. In his model he assumed the melt layer surface temperature to be equal to the particle temperature. Due to this assumption the effect of the particle thermal energy and the gas phase convection was found to be negligible. His results under predicted the experimental erosion results which were attributed to the inviscid nature of the hydrocode. Yang et al. [4,5] developed a model taking into effect the mechanical erosion and thermo-chemical ablation of the ablative layer. But they failed to account for the formation of the melt layer. They assumed that the particles impinge on the ablative surface and then bounce off. Later Cheung et al. [6] extended Yang's [4,5] model by taking into account the formation of the melt layer on the ablative

surface. They calculated the melt layer thickness near the stagnation region. In their study they found that the presence of the melt layer not only decreases the particle velocity and hence the mechanical erosion, but also acts as a thermal shield reducing the heat transferred to the ablative surface. But their model fails to account for the solidification of the alumina layer. Lewis and Anderson [2] developed a model taking into account both the solid and liquid alumina layer formation. In their model they assumed that when the liquid layer is growing the solid layer is of constant thickness and when the solid layer is growing the liquid layer is of constant thickness. Their model failed to account for the simultaneous growth of solid and liquid alumina layers and does not account for temperature variation of the thermo-physical properties. Their model results under predicted the experimental results for the ablation rate.

3. Present approach

In this work a transient, one dimensional heat transfer prediction model that includes the combined effect of melt layer formation and solidification is developed. The goal is to relate the heat transferred to the ablative surface to the parameters of the system i.e., particle mass flow rate, particle temperature, and gas heat flux. In formulating the model the variation of the thermo-physical properties with temperature is accounted for i.e., thermal conductivity and specific heat capacity. Also, the solid and the liquid layer are allowed to grow simultaneously, albeit at different rates. A finite volume approach is used in developing the model. The model uses a transformed grid to account for the mass influx and variable control volume size at the moving phase change interface. The control volume size near the solidification interface and the location of the interface is calculated using a Lagrangian interpolation technique. The model predicts the heat transfer effects inside a recirculation region where the shearing effect of the supersonic gas flow is small [2].

The intent of the present model is to understand the heat transfer to the ablative surface as influenced by the melt layer formation. The goal is a better understanding of the melt layer growth rates, the solidification process, and heat transport through the two phase layer. It is not intended to integrate the gas plume, melt layer and ablative layer heat transfer dynamics at this time. Aspects of ablative layer decomposition with resultant mass and heat transfer is not included. Any radiation effects from the gas plume are incorporated into the imposed melt layer heat flux at the melt layer surface. A more comprehensive model of the ablative process should eventually be coupled with both the ablative dynamics as well as the gas plume convective and radiative effects.

4. Development of physical and mathematical model

To facilitate mathematical formulation of the heat transfer problem, the following conditions are employed: (1) the fail temperature of the ablative layer (1600 K) is reached instantly and remains constant; (2) the effect of the shear stress due to the exhaust gas on the top of the melt layer is neglected; (3) there are no advection effects due to the pyrolysis gases from the ablative layer; (4) the solid/liquid interface temperature is at 2327 K (melting temperature of alumina) i.e., a fixed interface temperature and there is no mushy region; (5) the kinetic energy of the particles is fully converted into thermal energy; (6) the ablative surface is exposed to a constant average particle mass flow rate; (7) the gas phase applies a constant heat flux on the surface of the melt layer (this condition is valid during the initial stage of development where the temperature difference between the alumina and the gas plume is large); and (8) the process of heat transfer is treated as transient and one-dimensional.

Fig. 1 shows a schematic of the ablative layer exposed to a particle laden gas flow. Since the mass flow rate per unit area, $\dot{m}''_{\mathrm{p}}$, of the alumina particles is assumed to be a constant, the thickness of alumina deposited on the ablative layer during any time interval Δt is given as:

$$\delta_{\mathrm{n}} = \frac{\dot{m}''_{\mathrm{p}}\Delta t}{\rho} \tag{1}$$

The mass flux is taken as a range of typical values in a gas plume with particle sizes in the range of 1–100 μm, with a mean value of 11.7 μm. The associated average particle velocity is approximately 1650 m/s [4]. We choose to use the total mass flux as the parameter of interest in presenting the results while the kinetic energy associated with this flux is accounted for in the overall energy deposition, discussed later.

The temperature distribution in the deposited alumina layer, considering both the solid (s) and liquid (l)

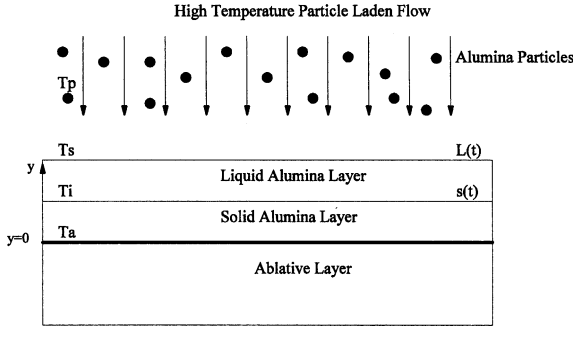

Fig. 1. Schematic of ablative layer exposed to particle laden flow.

layers, is governed by the transient one dimensional heat conduction equation [1]:

$$\rho_s c_{ps} \frac{\partial T_s}{\partial t} = \frac{\partial}{\partial y}\left(k_s \frac{\partial T_s}{\partial y}\right) \quad 0 \leqslant y \leqslant s(t) \tag{2}$$

$$\rho_l c_{pl} \frac{\partial T_l}{\partial t} = \frac{\partial}{\partial y}\left(k_l \frac{\partial T_l}{\partial y}\right) \quad s(t) \leqslant y \leqslant L(t) \tag{3}$$

In order to start the calculations, the initial condition assumes the presence of a very thin layer of alumina (0.1% of the total thickness at the end of calculations for the thinnest layer case). This layer is at a uniform temperature equal to the fail temperature (1600 K) of the ablative layer. The temperature at the alumina/ablative layer interface ($y = 0$) is a constant temperature boundary condition given by:

$$T(0,t) = T_a \tag{4}$$

At the gas/alumina interface ($y = L(t)$) a constant heat flux boundary condition is applied given by:

$$-k\left(\frac{\partial T}{\partial y}\right)_{y=L} = \dot{q}''_s \tag{5}$$

The magnitude of the outer surface heat flux is affected by different factors depending on whether the alumina layer is in the early phase or late phase of development; this is described in the following.

The early phase of alumina layer development is defined as the phase of development in which near instantaneous solidification of alumina occurs. This is due to the large temperature difference between the incoming alumina particles and the surface temperature of the alumina layer. Consequently, during this time only the solid alumina layer exists. Due to this near instantaneous solidification the latent heat released from solidification of alumina, the gas heat flux $\dot{q}''_{gas}$ and the kinetic energy $\dot{q}''_{KE}$ of the particles sum to equal the surface heat flux $\dot{q}''_s$ boundary condition.

$$\dot{q}''_s = \dot{q}''_{gas} + \dot{q}''_{KE} + \rho H \frac{\partial s}{\partial t} \tag{6}$$

The late phase of alumina layer development is defined as when the outer surface temperature of the alumina layer rises above the melting temperature of alumina so that both solid and liquid alumina layers coexist. With the solid and liquid alumina layers growing simultaneously, although at different rates, the Stefan condition should be satisfied at the solid/liquid alumina interface [1], which is given as:

$$-k_s\left(\frac{\partial T}{\partial y}\right)_s + k_l\left(\frac{\partial T}{\partial y}\right)_l = -\rho H \frac{\partial s}{\partial t} \quad \text{at} \quad y = s(t) \tag{7}$$

The heat flux boundary condition at the alumina/gas interface, $\dot{q}''_s$, for the late phase includes only the gas heat flux $\dot{q}''_{gas}$ and the kinetic energy $\dot{q}''_{KE}$ of the particles and is given by:

$$\dot{q}''_s = \dot{q}''_{gas} + \dot{q}''_{KE} \tag{8}$$

Since the particle thermal energy is released after the particle enters the melt layer, the thermal energy of the particles is directly added to the top of the melt layer and hence not included as a boundary condition. The thermal energy of the deposited alumina particles is based on a volume-averaged temperature. The averaged temperature is assigned to the new expanded grid at the top surface. This averaging uses the original volume of the top surface grid at the current time temperature and the added volume due to particle influx at its influx temperature.

Prior to formulating the finite volume equations, the coordinate system is transformed from the dimensional space and time coordinates, y and t, to the corresponding dimensionless variables ζ and τ. The dimensionless variables are defined as $\zeta = y/L(t)$ and $\tau = t/t_{ref}$, where $L(t)$ is the instantaneous thickness of the alumina layer. Since the reference length, $L(t)$, is time dependent, using this length to determine a reference time scale, $t_{ref} = L(t)^2/\alpha_o$, makes the problem indeterminate. Consequently, the reference time is made independent of the time dependent reference length by using an final time reference length, L_{ref} which is the layer thickness at the end of the calculations. The time used to calculate the reference length was chosen as the total time over which the calculation was to be executed, which is 5 s. Thus the reference time is constant throughout the calculation but the reference length is determined at every time step.

After coordinate transformation and using a continuous function for the thermo-physical properties, the non-dimensionalized governing equation is given by:

$$\frac{\partial \theta}{\partial \tau} = \frac{\alpha}{\alpha_o}\frac{L_{ref}^2}{L^2}\frac{\partial^2 \theta}{\partial \zeta^2} + \frac{1}{L}\frac{dL}{d\tau}\left[\frac{\partial \zeta \theta}{\zeta} - \theta\right] \quad 0 \leqslant \zeta \leqslant 1 \tag{9}$$

The solution of this equation along with the appropriate boundary and initial conditions results in the temperature distribution in the alumina layer. But the difficulty in solving the equation arises in accounting for the mass influx and tracking the solid liquid interface. To account for the mass influx two methods were identified. One procedure to expand the solution domain is to increase the number of control volumes. An alternative method is to keep the number of control volumes fixed but to increase the size of the control volumes as the mass is being deposited. In developing the numerical model a fixed number of control volumes with increasing size is used. This method is used for its reduced computational time and storage requirements. In the equivalent y coordinate the thickness of the alumina layer increases with time and accounts for the mass influx by increasing the size of the control volumes. But in the dimensionless

ζ coordinate the thickness of the alumina layer at any time is equal to unity. Employing a constant number of control volumes yields a non-dimensional spatial step size that is constant throughout the solution domain and independent of time.

The solution domain is divided into equally spaced control volumes and the general discretization equation for any arbitrary control volume is derived by integrating Eq. (9) over space and time. Using a piece-wise linear profile for the variation of temperature between grid points and a fully implicit method to march forward in time [7], the discretized governing equation is given by:

$$\frac{\rho c_p}{\rho_o c_{po}}(\theta_P-\theta_P^o)\frac{\Delta\zeta}{\Delta\tau}=\frac{L_{ref}^2}{L^2}\left[\frac{k_e}{k_o}\frac{\theta_E-\theta_P}{\Delta\zeta}-\frac{k_w}{k_o}\frac{\theta_P-\theta_W}{\Delta\zeta}\right]+\frac{1}{L}\frac{dL}{d\tau}\left[\frac{\rho c_p}{\rho_o c_{po}}\frac{(\zeta\theta)_E+(\zeta\theta)_P}{2}-\frac{\rho c_p}{\rho_o c_{po}}\frac{(\zeta\theta)_P+(\zeta\theta)_W}{2}-\frac{\rho c_p}{\rho_o c_{po}}\theta_P\Delta\zeta\right] \quad (10)$$

The subscripts W and E represent the west and east grid points respectively and the subscripts e and w represents the east and west control volume faces (see Fig. 2). The non-linearity caused by the variable thermo-physical properties is solved by letting the properties lag one time-step. The thermal conductivity at the control volume faces are calculated using the harmonic mean. Eq. (10) is a general equation for the internal grid points and it is suitably modified to account for the boundary condition.

When the multiphase layer begins to expand, the solid/liquid interface is tracked by having a variable control volume size near the interface. In this manner the interface is always located between two adjacent control volumes. To calculate the size of the control volume near the interface, and hence the interface location, the Stefan condition, Eq. (7), is used. The partial derivatives in the Stefan condition are approximated using the three point Lagrangian interpolation formula [1]. Since the interface location and temperature is known they can be used to specify a constant temperature boundary condition for those control volumes adjacent to the interface.

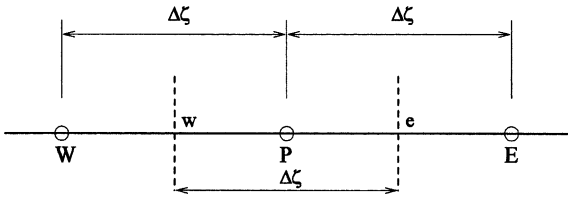

Fig. 2. Schematic of the grid points for the one-dimensional model.

5. Model verification

The model problem in this study does not have an analytical solution. The best way to assess this computational model is to suitably modify it to closely represent an analytical solution. The closest analytical solution available for this model is the Stefan problem [1]. For the computational model to closely resemble the Stefan problem, the mass influx was reduced to an insignificantly small value such that the solution domain does not noticeably expand between time steps. The initial condition for the computational model is such that there is sufficient amount of deposited material to establish the grid. The surface heat flux is also reduced to a very low value such that the heat flux does not affect the temperature distribution of alumina layer. To compare the solution of the computational model with the Stefan analytical solution an initial alumina layer thickness of 10 mm with a uniform temperature of 2800 K was used. A low mass flux of 1 mg/m^2 s was maintained. The maximum error of the temperature predicted by the numerical solution is less than 0.02% of the analytical result. This comparison helps to partially verify the accuracy of the computational model.

In addition, the model results were further evaluated for spatial step and time step convergence. The variation in temperature distribution for 100, 200 and 500 cells was analyzed and was found that the maximum error in temperature when the grid is refined from 100 to 200 cells is approximately 0.17%. Further refining the grid to 500 cells reduced the error to 0.10%. The temperature distribution for diffusion numbers 0.5, 0.1 and 0.01 for 500 cells was also studied. The change in temperature when the diffusion number is decreased from 0.5 to 0.1 was found to be about 0.023%. Further decreasing the diffusion number to 0.01 results in a temperature change of about 0.0006%. Based on these observations a diffusion number of 0.01 was used. Although the number of cells was fixed throughout the calculation procedure for any given mass flux, the number was increased linearly with the mass flux to maintain the same accuracy of the computational solution. Thus spatial and temporal convergence of the numerical solution was ensured.

6. Results and discussion

A total of 50 cases were evaluated to analyze the effects of particle mass flux, gas heat flux and particle temperature on the heat transfer process. A discussion of all these cases is given by Thirunavukarasu [8]. Table 1 gives the range of the system variables that were used.

All the particles are assumed to have a uniform velocity of 1650 m/s and the kinetic energy is calculated based on this velocity. The fail temperature of the ablative layer (1600 K), T_a, is used as the reference

Table 1
Test range for the system variables

Variables	Test range
Particle mass flux, $\dot{m}''_p$	1, 2, 3, 4, 5 kg/m^2 s
Gas heat flux, $\dot{q}''_{gas}$	1, 3, 5, 7, 9, 11 MW/m^2
Particle temperature, T_p	2400, 2600, 2800, 3000, 3200 K

temperature for the study and the reference thermophysical properties are evaluated at this temperature. An initial time step, Δt, of 1 ms was used to form the initial alumina layer for establishing the grid.

Table 2 shows the fractional distribution of energy at time $t = 0$ s for the base case conditions with $T_p = 2800$ K and $\dot{q}''_{gas} = 3$ MW/m^2 for various mass fluxes. The table shows the various sources by which energy is added to the system and the percentage contribution of each source to the heat transferred to the ablative surface. The gas heat flux, $\dot{q}''_{gas}$, is the primary source for lower mass fluxes. The particle kinetic energy, $\dot{q}''_{KE}$, and the particle thermal energy, $\dot{q}''_{part}$, increase almost linearly with mass flux. The latent heat released from solidification, $\dot{q}''_{lat}$, also increases with increasing mass flux and eventually, at high mass flux levels, it becomes a constant fraction of the heat flux to the ablative layer.

Fig. 3 shows the growth of the solid alumina layer, δ_s, for different particle mass fluxes. There is a linear solidification rate in the early phase of the alumina formation where only the solid alumina layer exists. The growth rate is obviously directly related to the mass flux of the particles. In the early phase of development the alumina layer is very thin and offers a minimal thermal resistance to the heat flow through the alumina layer. As the liquid alumina layer also begins to grow the solidification rate decreases. The time taken for the alumina to enter into the later phase decreases with increasing particle mass flux. This can be attributed to the larger time scale associated with the solidification rate compared to the deposition rate of alumina particles. Fig. 4 shows the relative solid layer growth rate $(\dot{m}''_s/\dot{m}''_p)$ with time. It can be observed that the solidification rate is consistently much lower than the particle deposition rate except for the lowest mass flux case at early times. This results in a relative thickening of the liquid layer over

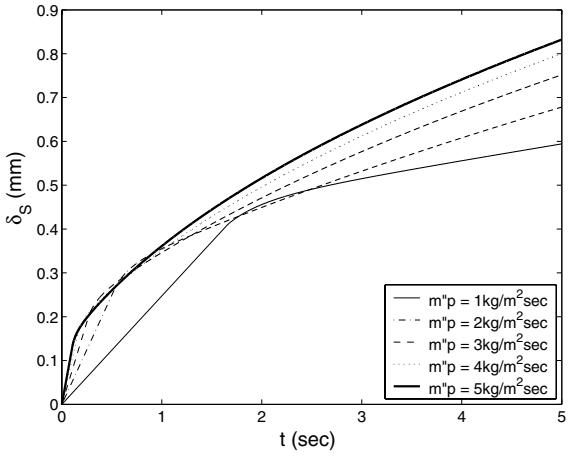

Fig. 3. Solidification growth rate for various mass flux for $\dot{q}''_{gas} = 3$ MW/m^2 and $T_p = 2800$ K.

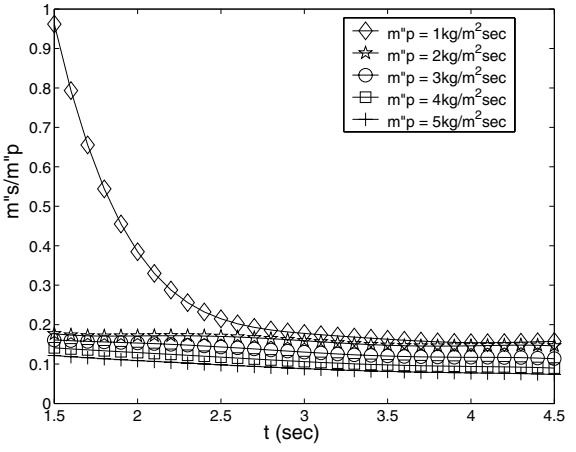

Fig. 4. Relative solid layer growth rate for various mass flux for $\dot{q}''_{gas} = 3$ MW/m^2 and $T_p = 2800$ K.

time. The ratio $(\dot{m}''_s/\dot{m}''_p)$ slowly decreases with time for all mass fluxes beyond 2.5 s.

The effect of gas heat flux on the relative solid layer thickness (δ_s/L) is presented in Fig. 5 for a particle

Table 2
Energy distribution for base case condition at $t = 0$ s

$\dot{m}''_p$, kg/m^2 s	1	2	3	4	5
$\dot{q}''_{ab}$, MW/m^2	7.01	10.985	14.925	18.785	22.55
$\dot{q}''_{gas}/\dot{q}''_{ab}$	0.428	0.273	0.201	0.159	0.133
$\dot{q}''_{KE}/\dot{q}''_{ab}$	0.194	0.248	0.273	0.29	0.30
$\dot{q}''_{part}/\dot{q}''_{ab}$	0.234	0.298	0.328	0.348	0.36
$\dot{q}''_{lat}/\dot{q}''_{ab}$	0.144	0.181	0.1966	0.201	0.202

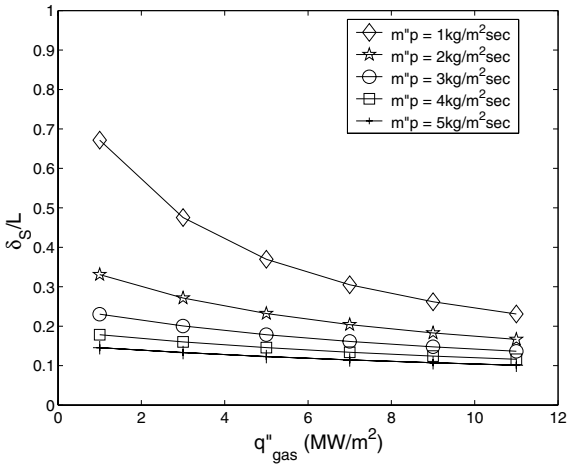

Fig. 5. Effect of gas heat flux on the relative solid layer thickness (δ_s/L) for $T_p = 2800$ K at time $t = 5$ s.

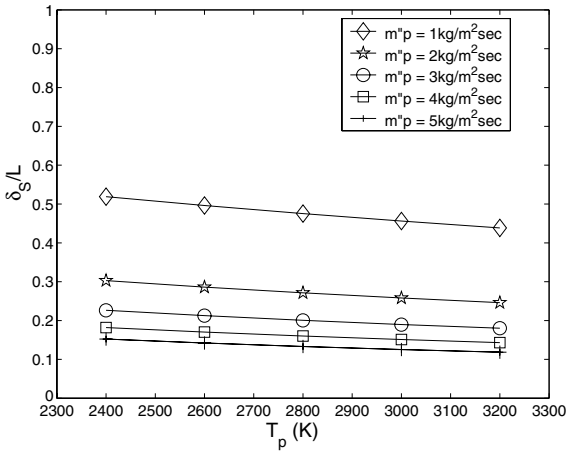

Fig. 6. Effect of particle temperature T_p on the relative solid layer thickness (δ_s/L) for $\dot{q}''_{gas} = 3$ MW/m^2 at time $t = 5$ s.

temperature $T_p = 2800$ K at time $t = 5$ s. The effect of the gas heat flux is found to be most predominant for the lower mass flux of 1 kg/m^2 s. For this low particle mass flux, the relative solid layer thickness decreases from 68% to 22% when the gas heat flux is increased from 1 to 11 MW/m^2. Increasing the gas heat flux increases the heat flux at the solid/liquid alumina interface. This increase in heat flux decreases the solidification rate. The effect of the gas heat flux decreases with the increase in the mass flux. For a higher mass flux of 5 kg/m^2 s the relative solid layer thickness decreases from 14% to 10% when the gas heat flux is increased from 1 to 11 MW/m^2. This small change compared to the low mass flux case can be attributed to a thicker liquid alumina. This thicker layer, due to its increased sensible storage, transfers less heat to the interface and the increase of $\dot{q}''_{gas}$ has a reduced impact on the solid layer thickness.

The effect of particle temperature, T_p, on the relative solid layer thickness (δ_s/L) is presented in Fig. 6 at time $t = 5$ s for a gas heat flux $\dot{q}''_{gas} = 3$ MW/m^2. As the particle temperature is increased the relative solid layer thickness (δ_s/L) decreases. This is because the heat flux to the solid alumina layer increases with particle temperature and causes the solidification rate to decrease. The effect of the particle temperature is approximately linear with nearly the same slope for all mass fluxes.

Fig. 7 shows the variation of the heat flux at the solid/liquid alumina interface with time. The heat flux at the solid/liquid alumina interface is the energy leaving the liquid alumina layer. This does not include the latent heat of solidification of alumina. It can be observed from the graph that the solid/liquid interface heat flux decreases with time. The heat flux at the interface decreases with time due to the development of the liquid

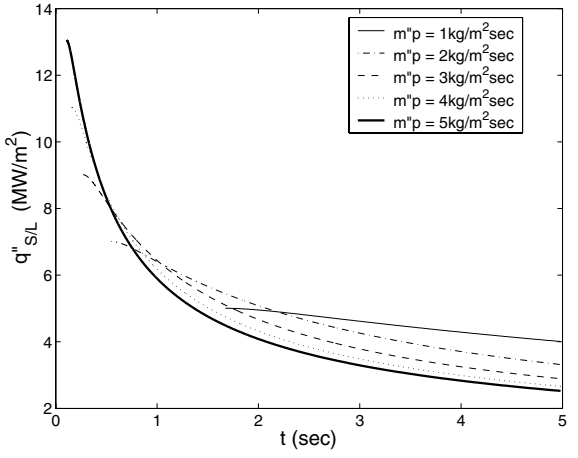

Fig. 7. Variation of heat flux at the solid/liquid alumina interface for $T_p = 2800$ K and gas heat flux of $\dot{q}''_{gas} = 3$ MW/m^2.

alumina layer. The rate of decrease of the heat flux at the interface depends on the particle mass flux. For the highest mass flux of 5 kg/m^2 s the interface heat flux decreases approximately exponentially from 13 MW/m^2 to as low as 2.5 MW/m^2 over 5 s, which is about a 81% decrease of the interface heat flux. For the lowest mass flux of 1 kg/m^2 s the heat flux decreases by 20%. A higher mass flux results in a thicker alumina layer which increases the sensible energy storage capacity and results in a reduced heat flux at the interface. Different starting times are observed for different mass fluxes in Fig. 7 since these results are meaningful only in the late phase of alumina layer development. A longer time is required to reach the late phase of liquid layer initiation for lower mass fluxes.

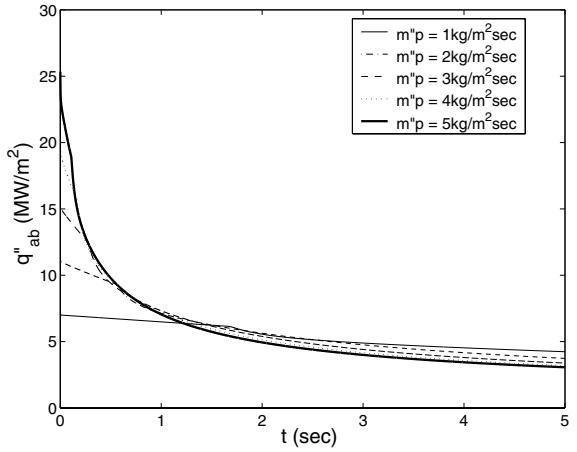

Fig. 8. Variation of heat flux to the ablative surface for $T_p = 2800$ K and gas heat flux of $\dot{q}''_{gas} = 3$ MW/m^2.

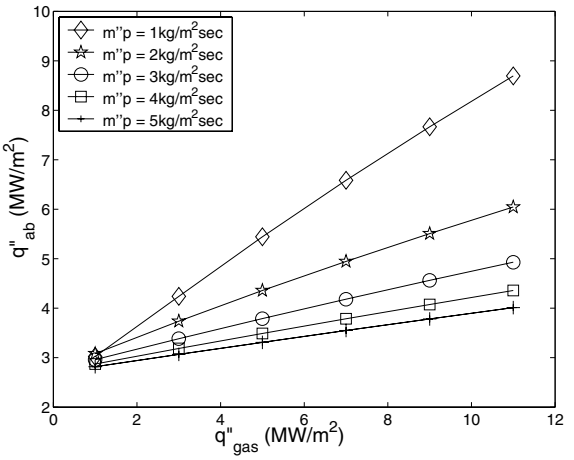

Fig. 9. Effect of gas heat flux on the heat flux to the ablative surface for a particle temperature $T_p = 2800$ K at time $t = 5$ s.

Fig. 8 presents the variation of the heat flux to the ablative surface versus time for a particle temperature $T_p = 2800$ K and a gas heat flux $\dot{q}''_{gas} = 3$ MW/m^2. The heat flux to the ablative surface decreases with the development of the alumina layer. During the early phase, the ablative surface is exposed to very high heat flux. As the alumina builds up on the ablative surface, the heat flux decreases drastically to values below 5 MW/m^2 after 2 s. Beyond this time results vary slowly. This shows that over time alumina particles, although, they impose a high heat flux during the initial phase, form a protective layer over the ablative surface and reduce thermal loading. The extent of this protection depends on the thickness of the alumina, and hence a higher mass flux of alumina particles tends to shield the ablative surface more effectively.

The heat flux to the ablative surface for a particle mass flux of 1 kg/m^2 s is reduced by 39%, over a time period of 5 s, by the development of the alumina layer. Increasing the particle mass flux to 5 kg/m^2 s, the heat flux to the ablative surface is reduced by 88% over the same time period. For this mass flux during the early phase of development where only the solid layer exists, the heat flux is reduced by 25%. But as soon as the alumina enters the later phase of development, where both the solid and the liquid alumina layers co-exist, the heat flux to the ablative surface is reduced by 66%. Fig. 8 also shows that the thicker liquid alumina layer, which is a result of higher mass flux, offers more thermal resistance than the solid layer. This is evident from the slope change in Fig. 8 when the liquid alumina layer starts growing. This can be attributed to two effects. One, there is a decrease in the thermal conductivity for the liquid of up to 38% due to the temperature variations in the liquid region from 2400 to 4200 K. Second, the thickness of the liquid layer becomes greater than the solid layer with higher particle mass flux cases having a higher thickness.

The effect of the gas heat flux on the energy transferred to the ablative surface is presented in Fig. 9 for a particle temperature $T_p = 2800$ K at time $t = 5$ s. It can be observed that as the gas heat flux increases the heat flux to the ablative surface also increases, essentially linearly. But for higher mass fluxes the rate of this increase is less due to a thicker liquid alumina layer. As an example, 21% of the 11 MW/m^2 gas heat flux supplied to the top surface does not reach the ablative surface for a mass flux of 1 kg/m^2 s versus 64% of the 11 MW/m^2 gas heat flux reaching the ablative surface for a mass flux of 5 kg/m^2 s.

Fig. 10 illustrates the effect of the particle temperature on the energy transferred to the ablative surface for a gas heat flux of $\dot{q}''_{gas} = 3$ MW/m^2 at time $t = 5$ s. Fig. 10 shows that the heat flux to the ablative surface increases linearly with the particle temperature. The slope is not affected by the mass flux, but the temperatures are significantly lower for higher values of mass flux. These linear effects can be attributed to the direct addition of particle energy to the alumina instead of applying it through a boundary condition.

The computational model for this study was developed to better understand the heat transfer characteristics associated with growth of solid and melt layer that occur in vertical missile launch systems. Experimental data from the missile launch systems is required to validate the results of this computational model. The model presented here imposes a constant heat flux boundary condition at the outer surface which simulates the gas interaction with the growth layer. In an actual system the gas flow over the ablative surface imposes a convective boundary condition, or a mixed thermal boundary condition. To use the mixed boundary con-

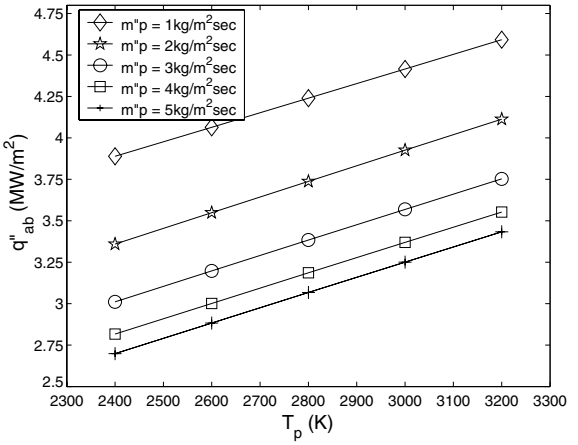

Fig. 10. Effect of particle temperature on the heat flux to the ablative surface for a gas heat flux $\dot{q}''_{\text{gas}} = 3$ MW/m^2 at time $t = 5$ s.

dition instead of the Neumann boundary condition, the properties and the conditions prevailing in the exhaust gas have to be known accurately. Due to the complexity involved in the high speed supersonic flow, the convective effects of the exhaust gas was neglected. The use of the Neumann boundary condition instead of the mixed boundary condition causes the temperature of the alumina to rise to high values, which might not be the case if a mixed boundary condition were to be used. In spite of this limitation of the model boundary condition, the Neumann boundary condition is justified for studying the heat transfer characteristics in the early stages of the alumina formation. This is because the surface temperature of the alumina is much lower than the gas temperature resulting in a high heat transfer rate equivalent to a Neumann boundary condition. The Neumann boundary condition is also justifiable in situations where the radiation heat effects are high and also in case of high mass fluxes where the particle kinetic energy is high enough to impose a constant heat flux boundary condition. Whether a constant heat flux boundary condition is used or a mixed boundary condition is used, the effect of the alumina is to protect the ablative surface, which is evident from the results presented.

The flow characteristics of a supersonic exhaust gas were investigated by Lewis and Anderson [2]. They reported that the exhaust gas forms a characteristic recirculation region, near the stagnation point, having very low shear stress values inside the region. In this region the alumina melt layer will not be smeared as it would further away from the stagnation region. Hence the computational model presented here is expected to more accurately predict the melt and solid layer growth rates and corresponding heat transfer in this stagnation region since the melt layer is not convected. The amount of particles entering this stagnation region depends on the size distribution of the particles. It was reported in the previous study [2], that only small size particles are carried along the gas flow path, where as the heavier particles impinge inside this stagnation region. Hence the predicted results of the computational model will be close to the experimental results if the particle distribution consists of larger size particles. In this region liquid and solid alumina layers tend to grow simultaneously as predicted in the model. The computational model can be extended to predict the heat transfer characteristics away from the stagnation region but with some error, which can only be found using experimental data.

7. Conclusion

A more accurate heat transfer model of the alumina layer was developed to study the solidification dynamics of simultaneous growth of solid–liquid layers. The model provides insight into the heat transferred to the ablative surface. The effects of the thermal loading, particle loading and temperature dependence of the thermo-physical properties of alumina are included in this investigation. The computational model was partially verified using an analytical solution to the Stefan problem. To further validate the computational model experimental data are required. It can be concluded that the particle mass flux is the major factor affecting the solidification growth rate of alumina and the development of the liquid alumina layer. However, the effect of the gas heat flux was found to have a major effect on the solidification dynamics for the lower mass fluxes. As the mass flux increases to higher values, the thermal resistance of the alumina layer also increases and helps to reduce the influence of the gas flux effectively. The particle temperature has a linear effect on the solid layer growth rate.

Acknowledgements

Partial funding for this project was provided through the Naval Surface Warfare Center with project monitor Leon Anderson and is greatly appreciated.

References

[1] J. Crank, Free and Moving Boundary Problems, Clarendon Press, Oxford, 1984.
[2] D.J. Lewis, L.P. Anderson, Effects of melt-layer formation on ablative materials exposed to highly aluminized rocket motor plumes, 36th Aerospace Sciences Meeting and Exhibit, Reno, NV, 1998, AIAA Paper No. 98-0872.

[3] G. Soo Hoo, Predictions of the Plenum floor erosion in the vertical launching system from a Mk 104 dual-thrust rocket motor restrained firing, NSWC TR-84-265, April 1985.
[4] B.C. Yang, F.B. Cheung, J.H. Koo, Numerical investigation of thermo-chemical and mechanical erosion of ablative materials, AIAA/SAE/ASME/ASEE 29th Joint Propulsion Conference and Exhibit, Monterey, CA, 1993, AIAA Paper No. 93-2045.
[5] B.C. Yang, F.B. Cheung, J.H. Koo, Modeling of one-dimensional thermo-mechanical erosion of high-temperature ablatives, Journal of Applied Mechanics 60 (1993) 1027–1032.
[6] F.B. Cheung, B.C. Yang, R.L. Burch, J.H. Koo, Effect of melt layer formation on thermo-mechanical erosion of high-temperature ablative materials, in: Proceedings of Pacific International Conference on Aerospace Science and Technology, National Cheng Kung University, Taiwan, 1993, pp. 302–309.
[7] H.K. Versteeg, W. Malalasekera, An Introduction to Computational Fluid Dynamics: The Finite Volume Method, Prentice Hall, Harlow, England, 1995.
[8] B. Thirunavukarasu, A study of solidification dynamics with liquid mass influx, M.S. thesis, Oregon State University, Corvallis, OR, 2003.